

CALIBRATION OF FAST FIBER-OPTIC BEAM LOSS MONITORS FOR THE ADVANCED PHOTON SOURCE STORAGE RING SUPERCONDUCTING UNDULATORS*

J. Dooling[†], K. Harkay, Y. Ivanyushenkov, V. Sajaev, A. Xiao, ANL, Argonne, IL 60439, USA
A. Vella, University of Illinois, Urbana-Champaign, IL 61801 USA

Abstract

We report on the calibration and use of fast fiber-optic (FO) beam loss monitors (BLMs) in the Advanced Photon Source storage ring (SR). A superconducting undulator prototype (SCU0) has been operating in SR Sector 6 (“ID6”) since the beginning of CY2013, and another undulator SCU1 (a 1.1-m length undulator that is three times the length of SCU0) is scheduled for installation in Sector 1 (“ID1”) in 2015. The SCU0 main coil often quenches during beam dumps. MARS simulations have shown that relatively small beam loss (<1 nC) can lead to temperature excursions sufficient to cause quenching when the SCU0 windings are near critical current. To characterize local beam losses, high-purity fused-silica FO cables were installed in ID6 on the SCU0 chamber transitions and in ID1 where SCU1 will be installed. These BLMs aid in the search for operating modes that protect the SCU structures from beam-loss-induced quenching. In this paper, we describe the BLM calibration process that included deliberate beam dumps at locations of BLMs. We also compare beam dump events where SCU0 did and did not quench.

INTRODUCTION AND MOTIVATION

The Superconducting Undulator Prototype (SCU0) is the first operating SCU in the APS storage ring (SR) [1]. SCU0 is installed in ID6 and has been producing photons for users since early 2013. The success of SCU0 has promoted the construction of SCU1. The length of the undulator in SCU0 is 0.33 m; in SCU1, the undulator length is 1.075 m. Often during beam dumps caused by the Machine Protection System (MPS), SCU0 quenches. Quenching inconveniences the x-ray users and potentially leads to magnet damage.

Simulations with MARS [2] have shown that relatively small beam losses (< 1 nC) can lead to temperature excursions sufficient to cause quenching when the SCU windings are near critical current. An initial model simulated a 1-nC, point beam of 7-GeV electrons striking the top of the vacuum chamber at the upstream end of the SCU0 magnet. With the beam starting upstream at the center of the chamber, this required a vertical angle of 4.3 mrad. Though unrealistically large, this beam trajectory allows a preliminary estimate of temperature rise within the SCU0 magnet windings for a given charge loss. Temperature excursions in the first 5 mm of undulator above the chamber are presented in

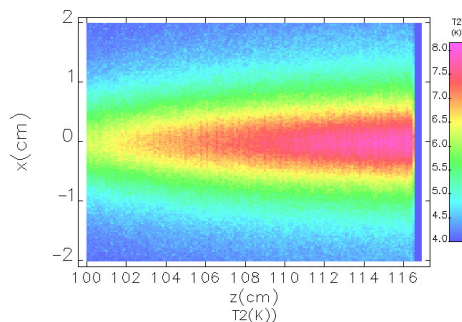


Figure 1: Temperature rise simulated in SCU0 after 1-nC of 7-GeV electrons strike the top of the vacuum chamber at the upstream end of the undulator ($z=83$ cm).

Figure 1 for an initial temperature of 4.2 K. Modeling with elegant [3] in other ID sectors shows that beam dumps deposit most of the beam on the upstream ID chamber transition section, making loss in the SCU0 undulator much more diffuse than indicated in Fig. 1. A temperature rise in excess of 1.9 K can lead to quenching at the SCU0 operating current of 500 A.

We present study and simulation results used to empirically calibrate the fast, fiber optic (FO) BLMs [4] installed in ID6. The calibration is then employed to evaluate losses recorded in ID6 caused by two separate beam dump events. In one case, the event did not lead to a quench of the SCU0 main coil, while in the other case, a quench did occur.

FIBER OPTIC BEAM LOSS MONITOR

Loss of primary, 7-GeV electrons leads to an electromagnetic (EM) shower composed of photons, electrons, and positrons. The high-purity, fused-silica fiber optic (FO) cable bundles are sensitive to all three of these EM shower components (in the case of photons, via pair production). Light is generated within the fibers via Čerenkov radiation as well as Optical Transition Radiation (OTR).

Experimental Description

Once light is generated within a fiber, the fiber provides a guide to an optical detector; in this case, Hamamatsu “sub-miniature” R7400 photomultiplier tubes (PMTs). Four fiber bundles are positioned in two pairs, one pair upstream of the SCU0 cryostat and the other downstream on the vacuum chamber transitions. The radiator ends of each bundle are placed parallel to the beam trajectory at the nominal beam centerline position; one bundle above and the other below

* Work supported by the U.S. Department of Energy, Office of Science, Office of Basic Energy Sciences, under Contract No. DE-AC02-06CH11357.

[†] dooling@aps.anl.gov

the vacuum chamber. Vertical separations between the individual bundles and beamline center are ± 5.4 cm on the upstream side and ± 2.8 cm on the downstream side. Each FO bundle is 4-m in length. The four PMTs are mounted within Pb-shielding on the floor of the SR tunnel.

Response times of the FO BLMs are determined by the PMT and the length of the fiber exposed to the EM shower. PMT rise time for the R7400 units are given as 0.78 ns [5]; this is sufficiently fast to observe most multi-bunch loss patterns within a single turn.

Loss Position Modeling

Using multiparticle tracking in *elegant*, a solution for isolating losses to ID6 is found with injection kicker IK2. Horizontal centroid position versus position around the storage ring (SR) is plotted in Figure 2. Also presented in Fig. 2 are FPGA BPM sum data which indicate the amount of beam loss at ID6. Good agreement is found between the measured and simulated loss locations in ID6. Results of

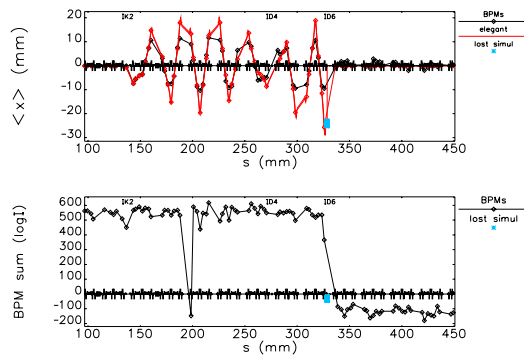


Figure 2: Top: horizontal centroid trajectories, comparing measurements (black) with simulation (red). Bottom: BPM sum signal and simulated loss location (blue). Machine parameters: injection kicker IK2 10 kV and *elegant* simulated kick 1.0 mrad.

the *elegant* model presented in Fig. 2 are supported by beam loss measurements in ID6 using the FO BLM.

Calibration Analysis

Calibration involves two measurement sets: 1) the relative gains of each channel employing a single light source, and 2) the absolute response on each channel with a known amount of lost charge.

For relative gain, an amber LED is coupled into the radiator end of the FO bundle. We want the four channels to respond equally to the same input signal. The channel scale factors are given in Table 1. The scale factors k_{pmt}

Table 1: PMT Response and Relative Gain

ID6 FO ch.	UT	UB	DT	DB
k_{pmt}	1.322	1.131	0.905	0.797

are used to equalize the response of each channel. The PMT output waveforms are recorded on a 500 MHz-bandwidth oscilloscope with a sample period of 800 ps and 0.5 MSample record length.

The integrated PMT output charge on channel j is

$$Q_{pmt,j} = \sum_{i=1}^{N_s} \frac{V_{i,j}}{R} \Delta t, \quad (1)$$

where N_s is the total number of samples, $R = 50 \Omega$, Δt is the sample period (typically 800 ps), and the PMT output voltage is defined as,

$$V_{i,j} = \begin{cases} V_{pmt,i,j} & V_{pmt,i,j} \geq V_{thres} \\ 0 & V_{pmt,i,j} < V_{thres} \end{cases} \quad (2)$$

with threshold voltage, V_{thres} . The data is fit versus intercepted beam current using a functional form that includes linear and saturation components [6],

$$Q_{pmt,j} = A_j \frac{I_j}{(1 + B_j I_j^{\alpha_j})^{1/\alpha_j}} \quad (3)$$

I_j represents the charge per unit time at detector j , where unit time is defined as the bunch period. The fits are forced to include the origin, ($I = 0, Q_{pmt,j} = 0$). This model accounts for the nonlinear response of the PMT detectors at high signal levels. When α^{-1} is an integer, Eq. 3 can be expressed as a polynomial. Substituting $u = BI^\alpha$,

$$Q(1+u)^{1/\alpha} = A \left(\frac{u}{B} \right)^{1/\alpha}. \quad (4)$$

For example, assuming $\alpha^{-1} = 3$, we obtain the cubic,

$$au^3 + bu^2 + cu + d = 0 \quad (5)$$

where,

$$a = 1, b = c = \frac{3QB^3}{QB^3 - A}, d = \frac{QB^3}{QB^3 - A} \quad (6)$$

For a given calibration data set, we first fit all three parameters A , B , and α using the SDDS toolkit command `sddsgenericfit` [7, 8] and select the closest integer value for α^{-1} . The data is then fit again keeping α constant to find the best values for A and B . Calibration is based on single-bunch loss; therefore, we apply Eq. 3 to the charge in each loss pulse. Having solved for I , the calibrated charge is expressed as,

$$Q_{cal,j} = k_j \tau_{QI} \sum_{p=1}^{N_p} I_{f,j,p}, \quad (7)$$

where the index p represents each loss pulse, k_j is the PMT correction factor from Table 1, τ_{QI} is the conversion of current to charge for one turn ($=3.68$ nC/mA), $I_{f,j,p}$ is the intercepted beam current from the fit associated with pulse p on channel j , and N_p is the total number of pulses. Results of fitting the calibration data are presented in Table 2 and plotted in Figure 3.

Content from this work may be used under the terms of the CC BY 3.0 licence (© 2015). Any distribution of this work must maintain attribution to the author(s), title of the work, publisher, and DOI.

Table 2: Fit of Single-bunch Deposition Calibration Data

j	α	A (nC/mA)	B (mA ^{1/α})
UT	0.393	91.579	1.931
UB	0.534	90.350	2.655
DT	0.300	80.840	1.417
DB	0.305	108.313	1.850

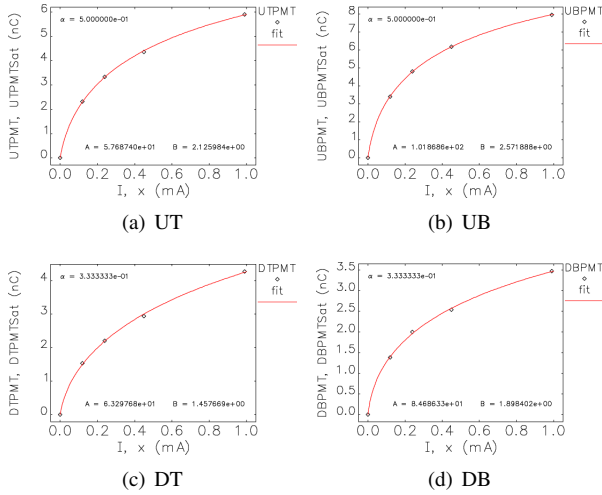


Figure 3: Direct deposition BLM data and fits in ID6.

DEPOSITED CHARGE IN ID6

With the calibration results presented above, we can estimate charge deposition in ID6 (SCU0). Two different loss events are compared, both of which were beam dumps that occurred during user operations in 2014; one event led to a quench and one did not. In both cases, the dumps took place with 100 mA and 24 evenly-spaced bunches. Examining autoscaled loss signals in a single turn shown in Figure 4, the bunch pattern is clearly resolved. Calibrated ID6 BLM data

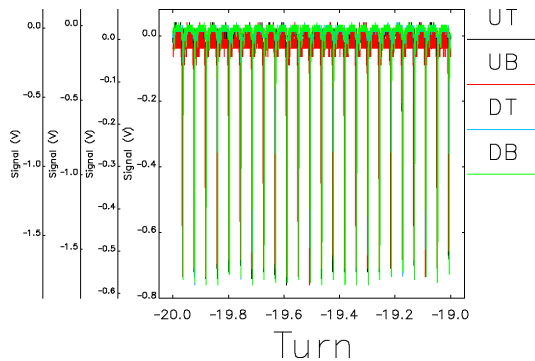


Figure 4: Expanding the loss signals over a single turn.

for the two beam dumps are presented in Figure 5. In both events, the SCU0 main coil current was set at 445 A which is 54% of the critical current. A Personnel Safety System (PSS) trip did not cause a quench of SCU0. The second

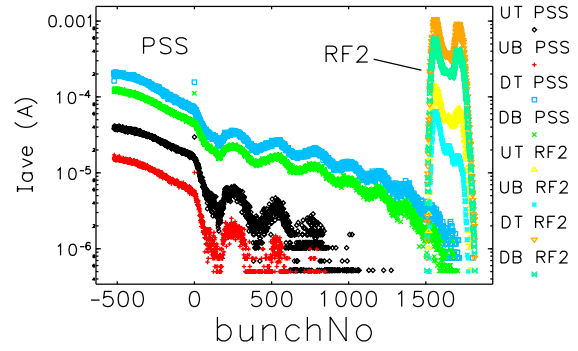


Figure 5: Average loss current for two beam dump cases. The RF2 trip did quench SCU0; the PSS trip did not.

event was due to an SR rf system 2 (RF2) trip; this loss did lead to a magnet quench. The average current shown in Figure 5 represents the calibrated charge per bunch period (153 ns) for the two beam loss cases. The PSS loss is spread over many tens of turns; on the other hand, the RF2 event is confined to just 10 turns. A comparison of measured and calibrated charge as well as maximum average current for the two beam dump cases is presented in Table 3.

Table 3: Loss Charge and Maximum Average Current for the PSS and RF2 Beam Dumps

j	PSS trip		RF2 trip	
	$Q_{cal,j}$ (nC)	$\langle I_{f,j} \rangle_{max}$ (mA)	$Q_{cal,j}$ (nC)	$\langle I_{f,j} \rangle_{max}$ (mA)
UT	2.724	0.041	2.398	0.142
UB	0.969	0.017	0.885	0.064
DT	15.228	0.213	19.999	1.062
DB	9.541	0.128	10.877	0.587
$\langle I_{max} \rangle$	—	0.100	—	0.464
$\sum_j Q_{cal,j}$	28.462	—	34.159	—

DISCUSSION AND FURTHER WORK

Calibrated BLM measurements indicate that beam loss charge greater than 1 nC may not always cause SCU0 to quench, suggesting the energy deposition is more diffuse than the simple, directed beam loss scenario described above. A more likely scenario is that primary, 7-GeV electrons first strike the transition section ≈ 1 m upstream of the SCU0 magnet [9]. Also, the loss time scale may be a factor. Local beam loss measurements have allowed us to quantify charge lost in the SCU0 and test methods for directing beam dumps away from the device [10].

ACKNOWLEDGMENTS

The authors thank Adam Brill, Chuck Doose, John Grimmer, and his staff for installation of the FO BLMs.

REFERENCES

- [1] Y. Ivanyushenkov et al. *Phys Rev ST Accel Beams (in press)* (2015).
- [2] N. V. Mokhov et al. Fermilab-Conf-07/008-AD; AIP Conf. Proc. 896, FNAL (2007).
- [3] M. Borland. ANL/APS LS-287, Advanced Photon Source (2000).
- [4] J. Dooling et al. *Proc. of PAC 2009*, 3438–3440 (2009).
- [5] Metal Package Photomultiplier Tube R7400U Series, TPMH1204E07 (2004). http://ctf3-tbts.web.cern.ch/ctf3-tbts/instr/PMT/R7400U_TPMH1204E07.pdf
- [6] L. Emery. Private Communication, August 2014.
- [7] M. Borland et al. User's Guide for SDDS Toolkit Version 2.8 (January 28, 2014). http://www.aps.anl.gov/Accelerator_Systems_Division/Accelerator_Operations_Physics/manuals/SDDStoolkit/SDDStoolkit.html
- [8] R. Soliday et al. *Proc. of PAC 2003*, 3473–3475 (2003).
- [9] J. Dooling et al. *Proc. of IPAC 2012*, 106–108 (2012).
- [10] K. Harkay et al. *These Proc. (TUPJE066)* (2015).